6.1 Introduction

Organic photovoltaics devices are considered as encouraging technology that may be the next generation flat-panel display platform for environment-friendly renewable energy resource [Heo et al. (2011)]. Variety of processing strategies and approaches has been adapted to improve the polymer-based photovoltaic devices which include a better understanding of the device physics, new materials for high performance, optimization of the morphologies by advanced processing methods, and advanced device architectures [Liu et al. (2014), Zhang et al. (2016)]. However, the cost and output of these devices are not yet up to the benchmark of commercialization level, and further improvement is naturally essential for large-size applications by using roll-to-roll manufacturing methods. Therefore, one approach to improve the efficiency of polymer-based photovoltaic devices such as solar cells (PSCs), photodetector is to stimulate photon absorption inside the organic thin film via surface plasmon resonance (SPR) [Heo et al. (2011), Zhang et al. (2016), Chou et al. (2014)]. It can be a practical approach to enhance the photo-generation of excitons via light trapping by increasing the photon absorption efficiency of the organic materials with the incorporation of plasmonic nanomaterials in the photovoltaic devices while retaining their optical thickness [Chou et al. (2014)]. π- conjugated organic semiconductors with metal nanoparticle open new opportunities and provide a path to tailor their self-assembly and electronic properties to contest particular application demands.

Surface plasmons are waves associated with strongly enhanced electromagnetic fields on the surface due to their interaction with the free electrons of certain metals, such as gold, copper, silver, and their alloys [West et al. (2010), Lee et al. (2006), Link et al. (1999)]. So metal nanoparticles (NPs) [Moores et al. (2006), Sardar et al. (2009)] have played the prominent role because of its extraordinary optoelectronic properties which particularly

ascend due to the collective oscillation of electron density (surface plasmons induced) at the large surface of NPs [Wu et al. (2011), Walters et al. (2009)]. Such properties of metal nanoparticles of exhibiting efficient absorbance as well as scattering, may be effectively utilized into photonic and electronic device applications. However, metal nanoparticles are liable to form its aggregate in solution [Moores et al. (2006]. So it's a research enthused case of study to link the metal NPs to conjugated polymers by a synthetic approach using polymeric stabilizing species. As it is a well-known fact that metal NPs are bound physically or chemically to a polymer in polymeric vesicles (core-shell) [Kuila et al. (2017)].

Metal nanoparticles (NPs) have attracted much consideration because of their excellent optoelectronic properties [Noguez (2007), Biju et al. (2008)]. Such optical properties arise from surface plasmons induced by the collective oscillation of electron density at the large surface of NPs [Moores et al. (2006), Sardar et al. (2009)]. The efficient absorbance and scattering of light of the metal nanoparticles may be utilized in electronic and photonic devices [Kuila et al. (2017), Moores et al. (2006), Sardar et al. (2009)]. In spite of this, the interaction behaviour of organic molecules and metal nanostructures is highly reliant on the electronic structure of the same. As compared to other noble metals, silver metal nanostructures exhibit fertility in surface plasmons which are confined and localized in nanoscale systems [Amendola et al. (2010)]. This nanoscale confinement of surface plasmons permits the conjugation of metal nanostructures with organic semiconducting molecules, which ultimately caused by its highly flexible introduction in tailoring the localized plasmonic properties [Jiang et al. (2014), Pandey et al. (2015)].

Thus, despite of such strong potential for improvement of the device performance and efficiency based on metal nanostructures, a few numbers of report available offering the improvement in spectroscopic as well as charge transport properties [Pandey et al. (2015)].

Recently, poly (3, 3′′′-didodecylquarterthiophene) [PQT-12] a solution processable polymer for organic devices has received astonishing attention of researchers. The prolonged π-conjugation facilitated by the presence of long dodecyl chain on the polymer backbone makes it a suitable semiconductor material. It also shows solution processability, molecular self-organization, and liquid crystalline property. The highly regular chain structure causes film form lamellar structures with interchain stacking through self-organization into two-dimensional sheets, which is confirmed by X-ray diffraction (XRD) and scanning tunneling microscopy (STM) study. These properties of rr-PQT-12 represent excellent organic device characteristics and make them a model material for easy fabrication of large area electronic devices [Singh et al. (2017), Pandey et al. (2017), Pandey et al. (2015), Facchetti (2010), Liu et al. (2011)].

This report aims to demonstrate the simple strategies for the synthesis of phase transferred Ag nanoparticle and Ag NPs@rr-PQT-12 nanocomposite large area thin film over high surface free energy liquid substrate for photovoltaic application. Prior to deposition and investigation of nano-composite thin film, synthesis of phase transferred Ag nanoparticles in chloroform was characterized using multiple techniques. The nucleation and growth phenomena of these composite thin films over high surface free energy liquid substrate were discussed in detail. In order to validate the synthesis of Ag nanoparticle's surface plasmons and conjugated polymer excitons coupled thin film, multiple characterizations such as HR-TEM, AFM, spectral, and structural characterization were carried out. Finally, the

photovoltaic property of polymer nano-composite film was investigated under the illumination of different wavelength of light, which demonstrates the wavelength dependent photoconductivity. Thus, our study has demonstrated a path for fabrication of large area polymer nanocomposites thin film with the enhanced photovoltaic property.

6.2 Experimental

6.2.1 Materials

Didodecyldimethylammonium bromide (DDAB), silver nitrate (anhydrous) and sodium borohydride were purchased from Aldrich Chemicals Co., USA. rr-PQT-12 (ADS12PQT, Lot#14K007B1, molecular weight = 15,000–50,000 & HOMO = 5.24 eV & LUMO = 2.97 eV) was purchased from American Dye Source, Inc. USA and chloroform (analytical grade), ethylene glycol (EG) and glycerol were obtained from Merck, India and used without further purification. Double distilled deionized ultra-pure water was used in all experiments.

6.2.2 Preparation of stabilized Ag NPs/rr-PQT-C12 composite

Prior to stabilized Ag NPs/rr-PQT-C12 composite formation, the AgNPs are synthesized through reduction of silver salt with sodium borohydride in aqueous medium as reported somewhere else [Mishra et al. (2017)]. In brief, freshly prepared aqueous silver nitrate solution (10 mL, 0.001 M) is added to ice cooled aqueous sodium borohydride (30 mL, 0.002 M) solution with continuous stirring (1100 rpm) at rate of one drop per second. The final dark yellow solution obtained is AgNPs in aqueous solution. In order to transferee these AgNPs to chloroform, DDAB (5 mL, 5 mM) already dissolved in chloroform, is exploited as phase transfer agent into the organic medium. These phase transferred NPs obtained are in the size range of 7-12 nm and utilized further for decoration into polymer matrix.

rr-PQT-12 (0.5 % w/v) is added to the freshly prepared silver organosol (mL) followed by shaking on mechanical vibrator to ensure its proper mixing. This solution was explored in order to form large area nanocomposite thin film utilizing the surface energy gradient over liquid substrate which has been discussed in detail in later section.

6.3 Results and discussion

(a) Characterization of Ag nanoparticle

In order to validate the formation of Ag NPs in hydrosol, and phase transfer of same from hydrosol to organosol (chloroform), UV-vis absorption spectra were recorded in different medium as shown in Fig. 6.1. It is important to mention here that silver nanoparticles in aqueous and organic medium were ascertained for its surface plasmon resonance (SPR) via UV-vis studies. Both solutions viz hydrosol and organosol revealed SPR (Fig. 6.1) absorptions with some difference in wavelength. Hydrosol shows its λ_{max} at 387 nm, whereas same nanoparticles phase transferred into chloroform depict a red shift (408 nm) attributed to change in chemical environment. All nanoparticles synthesized in aqueous could not be transferred into the organic medium which can be seen with evidence of change in intensity of curves hydrosol and organosol. During phase transfer some bigger particles are sustained in the aqueous phase as DDAB does its excellent job of being a size sorter at the liquid-liquid interface. These narrow and uniform sized particles are expected to be dispersed uniformly throughout the polymer matrix.

Further, in order to examine the shape, size and crystallinity, TEM, HR-TEM and SAED were recorded, Ag NPs obtained from both media as shown in Fig. 6.2. TEM image recorded for hydrosol Ag NPs shows the formation of NPs ranging from few nanometers to few tens of nanometers. However, TEM image of organosol reveals the NPs ranging upto 10-12 nm

only which validate the results obtained from UV-vis. HR-TEM image of same NPs shows the fringes of plane with inter planner spacing 0.22 nm which correspond to (111) plane. The appearance fringes of plane confirms the formation of highly crystalline Ag NPs. SAED pattern of same NPs further demonstrate the formation of multidirectional oriented crystalline NPs.
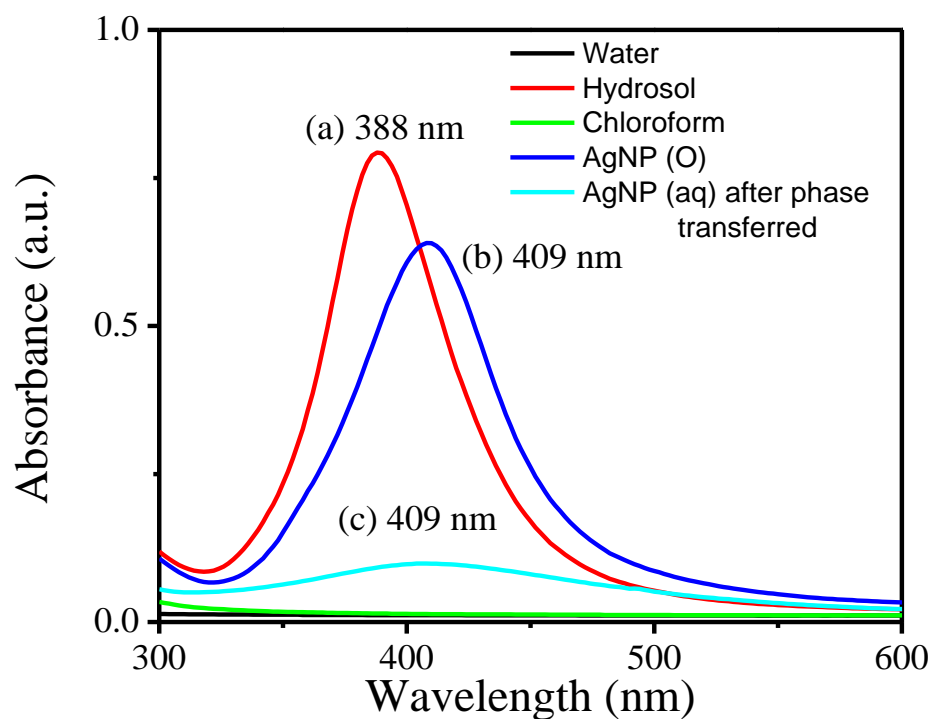

Fig. 6.1. UV-vis spectra depicting SPR of hydrosol, silver nanoparticles in chloroform (after phase transfer) and, silver nanoparticles retained in aqueous phase (after phase transfer)
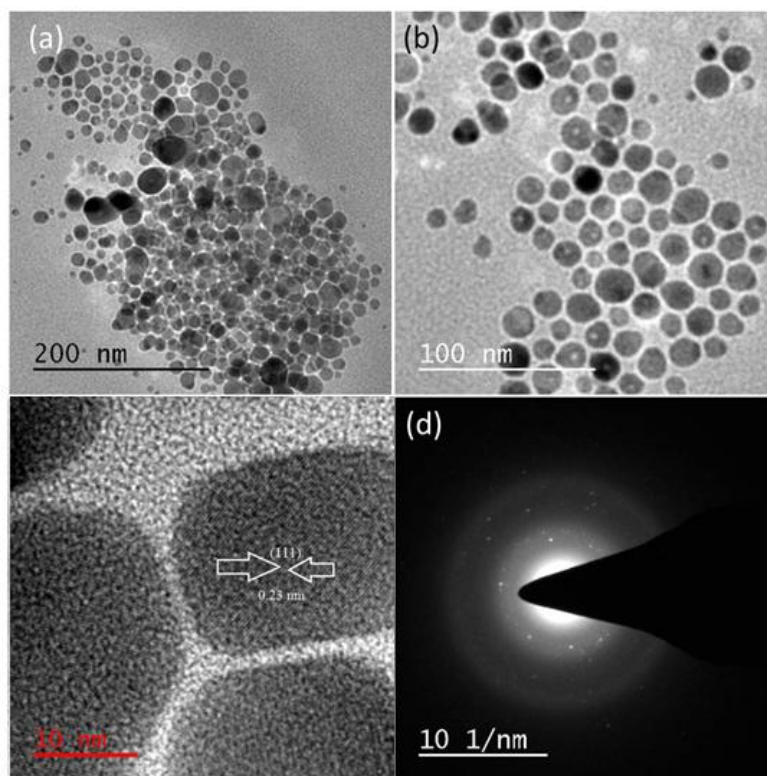
Fig. 6.2. TEM images of (a) Hydrosol, (b) Organasol (after phase transfer), (c) HR-TEM image of organosol (after phase transfer), & (d) SAED image of organosol

Nucleation and growth phenomena of rr-PQT-12 coated Ag nanoparticle thin film:

The fabrication of thin film followed by the development of silver nanoparticles (AgNPs) decorated polymer matrix (rr-PQT-12) (schematically shown in Fig. 6.3 (a)) was done as described in experimental section. During the fabrication of thin film based upon specific technique, one must know the importance of spreading coefficient which is playing a vital role in formation of thin film. This spreading coefficient portrays the contrast between the work of attachment and the work of cohesion of a fluid spreading on a surface.

The calculation of spreading coefficient of any solvent onto a liquid surface can be obtained by the equation: $S = \gamma_{liq} - \gamma_{sol} - \gamma_{liq-sol}$, Fig. 6.3(b) outlines the arrangement of nanohybrid thin

film at air fluid interface, facilitated by means of surface tension gradient of water, Compressive Force (CF) and viscosity of base fluid. It is critical here to specify that there are two parameters such as surface pressure slopes and thickness of base fluid which plays an imperative part within the arrangement of adjusted polymer film.
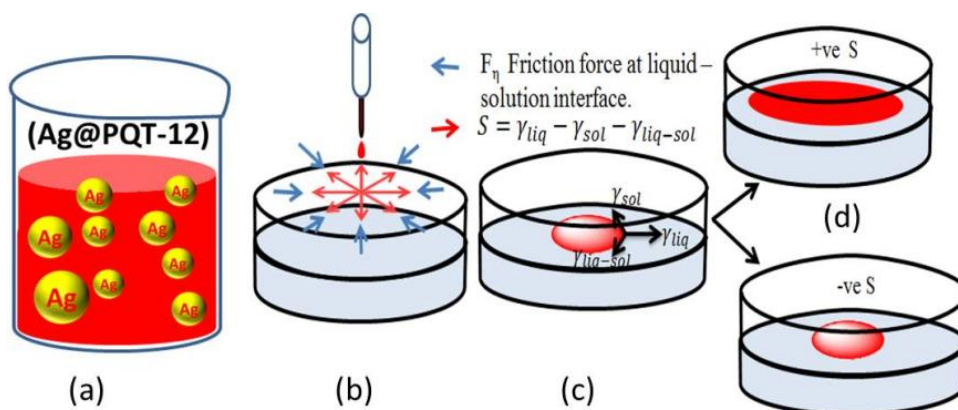

Fig. 6.3 (a) Schematic representation of Ag NPs dispersion into rr-PQT-12, (b) representation of the precise growth of Ag@PQT-12 (AgNPs@rr-PQT-12) thin film on the surface of high surface tension mobile liquid substrate accomplished by surface tension gradient and compressive force (c) surficial flow of hybrid solution on the liquid substrate (d) Illustrations of formation of Ag NPs decorated rr-PQT-12 in S>0 and S<0.

It is imperative here to specify that there are two parameters such as surface tension gradient and viscosity of base fluid which plays a critical role within the arrangement of oriented polymer film. The generation of local surface tension gradient leads towards the boundary between the encompassing materials when the low-surface tension solvents like hydrocarbons are dripped over high-surface tension surfaces like hydrophilic surface. Due to this; the low-energy solvent starts flowing towards high surface tension regime along the surface and this mechanism is called Marangoni flow.

Hence, in our case also this mechanism has been in effect as nanohybrid based polymer i.e. AgNP/rr-PQT-12 (low surface tension solvent) has been dropped over lyophilic surface (high

surface tension). Here again spreading coefficient comes into the force to decide the direction of flow of low energy solvents. This spreading coefficient(S) is defined as per earlier equation i.e. S= γ_1-γ_2-γ_{12} (where, γ_1 and γ_2 denotes the surface tensions of the mixture and composite solutions, respectively, and γ_{12} represents the interfacial surface tension of the two liquid as shown in Fig. 6.3 (c)). For proper spreading of the polymer solution over the liquid surface, there must be a positive 'S', i.e. γ_1 ; the surface tension of the base solution must be larger than the sum of γ_2 and γ_{12} ; the surface tension of the polymer solution. The negative 'S' indicates that the polymer solution is unlikely to spread while the extent '$S^{1/2}$' portrays the spreading speed for the same. In our case; we have obtained the positive 'S' thus it can be refereed as spontaneous spreading flow would be exhibited by $CHCl_3$ only. It is additionally essential that Ag NPs decorated polymer gets well oriented amid spontaneous spreading flow of solution. The formation of compact self-assembled polymer thin films is mainly due to the optimized ratio of hydrophilic liquid substrate and evaporation rate of $CHCl_3$ at room temperature. Fig. 6.3 (d) outlines the schematics for the arrangement of a polymer nano-composite film on an fluid substrate with +S. (i) At first, the nano-composite arrangement is dropped onto the lyophilic (fluid) substrate and arrangement rapidly spreads exterior as demonstrated by arrow due to + S inside division of moment (ii) since the chloroform dissipates exceptionally quickly, the drying process happens momentarily to create an oriented, profoundly situated thin solid polymer nano-composite layer on the fluid substrate; (iii) this thin film can promptly be exchanged to an assortment of target substrates, by stamping the substrates on the nanocomposite film.

(b) Characterization of nanohybrid film

Morphological Characterizations:

In order to interrogate the distribution of Ag NPs in polymer matrix, effect of Ag NPs on morphology, TEM were carried out as shown in Fig. 6.4. TEM image of composite reveals the uniform distribution Ag NPs in polymer matrix. However, HR-TEM of Ag NPs shows the fringes of Ag plane with inter planner spacing 0.22 nm which correspond to (111) plane.
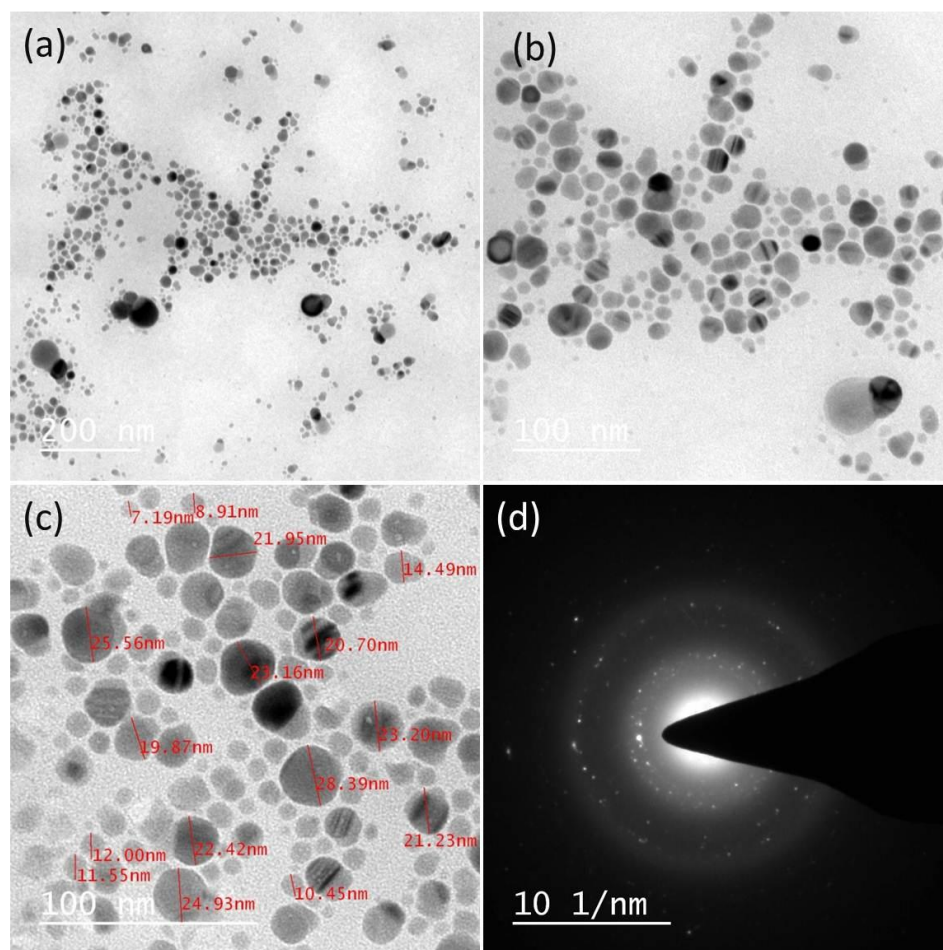

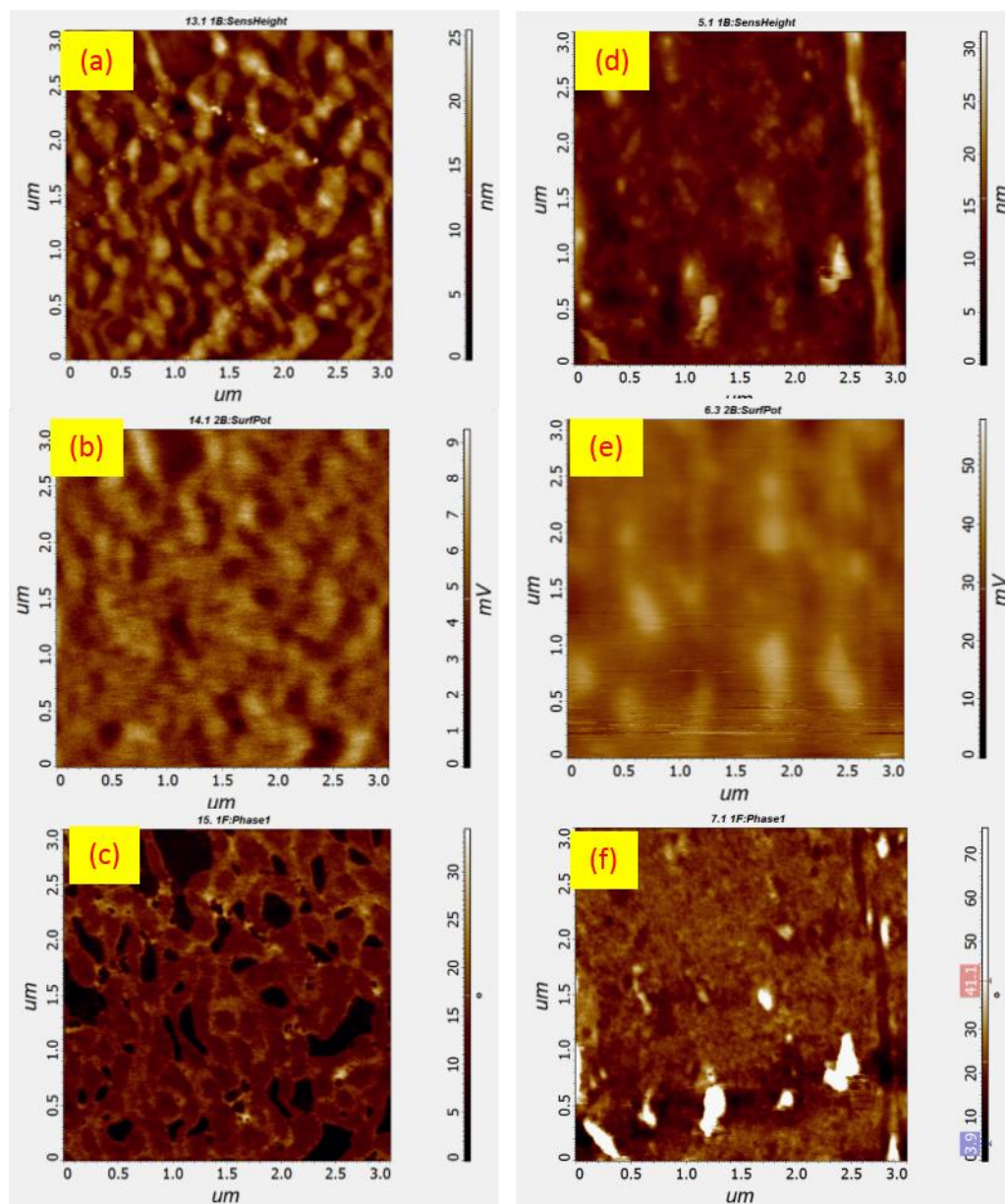**Fig. 6.4.** TEM images (a, b & c), size distribution & (d) SAED image of AgNP@rr-PQT-12.

Fig. 6.5. AFM (a) height, SPC and phase contrast image of (a-c) pristine rr-PQT-12 and (d-e) AgNPs@rr-PQT-12 based polymer films.

The atomic force microscopy (AFM) characterization was done for the topographical analysis of FTM deposited PQT as well as Ag NPs@rr-PQT-12 based thin films. The height, surface potential and phase of the both sample was observed (*cf.* Fig. 6.5). Both films show the fibrous structure which is also confirmed from its respective phase images. Further, the surface potential contrast investigation of both films via kelvin probe force microscopy

(KPFM) by providing 3V of bias voltage to the ITO substrate reveals the different morphology. From the KPFM image, it is clear that the surface potential of Ag NPs@rr-PQT-12 FTM film is ~ 5 fold enhanced as compared to that of rr-PQT-12 FTM film, due to incorporation of silver nanoparticles (AgNPs) into rr-PQT-12 matrix.
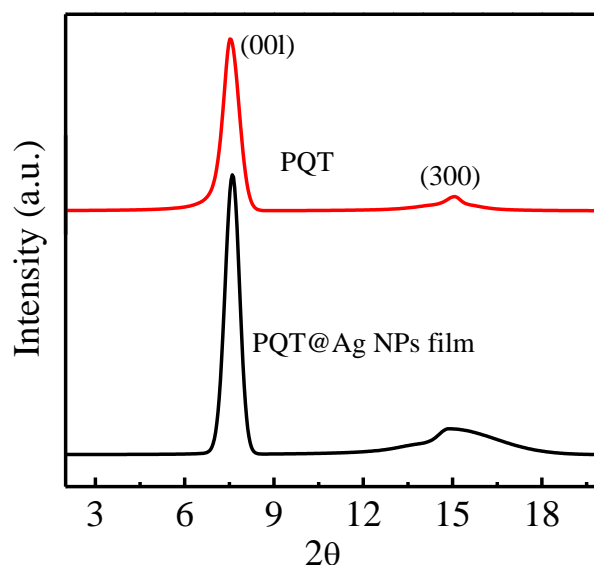
Structural Characterizations:

Fig. 6.6. GIXD of Ag NPs@rr-PQT-12 and pristine rr-PQT-12 film formed over high surface energy liquid substrate.

In order to examine the effect of Ag NPs on structural property, we carried out GIXD at 0.2^0 grazing angle which was equipped with inplane diffractometer and out of plane moving detector and compare with pristine polymer film. The GIXD patterns of the pristine PQT as well as Ag NPs@rr-PQT-12 thin films showed single, very distinct crystalline peak at $2\theta = 7.4^0$, indicative of formation of oriented crystalline polymer film in both case. However, there is absence of peaks corresponding to Ag NPs, indication of presence of less amount of Ag NPs (<3%). Further, the inter planner spacing calculated using formula $2d_{001} \sin\theta = n\lambda$, (where d_{001} stands for (001) inter planner spacing) and found to be ~1.2 nm. This spacing

is arises due to ordering of the alkyl side-chains from the cofacial π-π stacking of the polymer chains, in excellent agreement with the theoretical estimation presented by Ong et al. [Ong et al. (2005), Maillard and Rochefort (2009)]. In previous section, it has already been confirmed via SAED about existence of (010) plane with inter planner spacing 0.38 nm, corresponding to a typical face-to-face π-π stacking for polythiophenes. In order to calculate the structural coherence length L_c attributed to crystalline domains along (001) direction, Scherrer's formula $L_c = \frac{0.9\lambda}{FWHM cos\theta}$ was explored. Although, this relation is usually explored for estimation of crystallite size but due to directional growth in polymer crystallites, it is difficult to estimate accurate crystallite size. Therfore, we designated it as L_c and are used to compare the crystallite sizes present in both samples. It is found to be 17.3 nm and 14.8 nm for Ag NPs@rr-PQT-12and pristine PQT, respectively. The (0k0), and (h00) diffraction peak, corresponding to the π–π stacking and alkyl chain of polymer backbones, is not appeared in GIXD. The absence of these two plane peaks in film arises due to formation of highly head on oriented polymer film. It is noteworthy here that we have recorded spectra at fixed grazing angle 0.2 of X-Ray with respect to both film during recording and detector moves out of plane with angle 2θ. The schematics of GIXD measurements, selected throughout the recording of spectra, have been demonstrated in Fig. 6.6, where movement of detector and scattering vector χ is out of plane to the film surface. However, X-ray beam is kept at fixed angle 0.2 and in plane of film surface. Due to this, X-ray beam interact only with certain fixed plane i e. (00l) only in our case throughout the out of plane movement of detector. This causes the appearance of (00l) set of plane only. Thus, in our case, we acquire head on oriented, highly crystalline thin film of polymer which is highly desirable for out of

plane device, fabricated in sandwiched structure because maximum charge transportation occurs along either polymer backbone or π-π stacking direction.

Surface enhanced Raman scattering study:

Furthermore, in order to interrogate the effect of Ag NPs at polymer vibrational spectral property, surface enhanced Raman scattering was carried out to both film viz. Ag NPs@rr-PQT-12 and compare with pristine PQT polymer film of same thickness as shown in Fig. 6.7. Both films demonstrates peaks at 1455 cm^{-1} (major peak), 1390 cm^{-1} 1057 cm^{-1} and 687 cm^{-1} correspond to C=C symmetrical stretching, ring C–C stretching, C–H bending vibrations, and C-C alicyclic/aliphatic chain vibrations (medium) respectively. On comparing the peak intensity of both samples, it was detected that Ag NPs@rr-PQT-12 film shows extremely strong Raman peaks at the respective positions compared to that of rr-PQT-12 based film. Nearly, a nine fold enhancement is observed in C=C symmetrical stretching mode (1455 cm^{-1}) of Raman signal. The magnitude of enhancement in Raman signal of Ag NPs@rr-PQT-12 vibrations in this case is very less (~9 fold) in comparison with electromagnetic near field effect for isolated system (should be nearly 1000 fold) [Otto (2005)]. This again indicates the formation of plasmon coupled fluorophore unified system due to adsorption of the silver nanoparticle incorporated into rr-PQT-12 (Ag NPs@rr-PQT-12) FTM film. It is probably because of a chemical enhancement of surface plasmon enhanced Raman signals by inter molecular interaction [Pandey et al. (2015)].
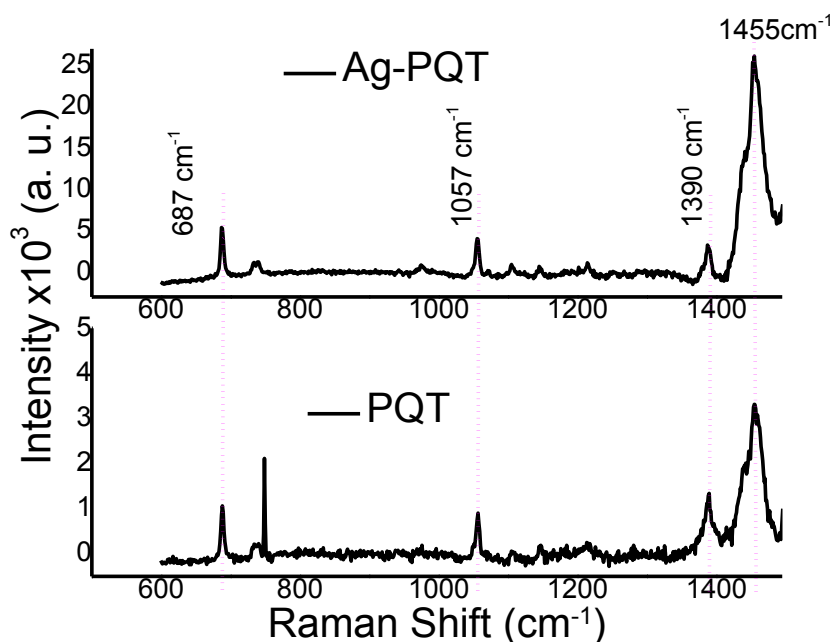
Fig. 6.7. Raman spectra of pristine rr-PQT-12 and AgNPs@rr-PQT-12 film, respectively.

Fabrication of device and study of photovoltaic properties:

Finally, in order to examine the effect of Ag NPs on photovoltaic property of polymer, sandwiched structure of ITO/Ag NPs@rr-PQT-12/Al schottky devices(schematically shown in inset of Fig. 6.8) was employed under illumination of different wavelength of light. It is noteworthy here that all devices were illuminated from ITO side and photo response was recorded in reverse bias mode of schottky device. The dark current (in absence of light) in the case of Ag NPs@rr-PQT-12 based Schottky device is of the order of few hundreds micro ampere. However, illumination of device from back side demonstrates wavelength dependent current density. Maximum current were observed for green light. However, Red and green light demonstrate lesser current density as compare to green light. It is important to mention here that red, blue and green light enhance current density upto 60 to 70 fold as compare to dark current as shown in the Fig. 6.8. Such a high response can be explained via in terms of coupling of Ag NPs and conducting polymer exciton and spectral band width

of Ag NPs@rr-PQT-12. It is important to note that most part of electronic absorption spectrum of Ag NPs@rr-PQT-12 fall in the range blue green and red. In our case, we have also incorporated the Ag NPs in polymer matrix. It is important to mention here that electric field generated by NPs is localized and organic molecule away from NPs does not affect from localized field. Therefore, incorporation of Ag NPs effects the nearer organic molecule mostly. Thus, presence of Ag NPs and highest electronic absorption between among these three color causes such a high photo current. Therefore, in our case, we get such a high response of our materials.

Further, in order to understand the enhancement in spectral as well as photovoltaic current Ag NPs@PQT film, XPS measurement of AgNPs@rr-PQT-12 and pristine rr-PQT-12 were carried out. XPS spectra of Ag NPs@rr-PQT-12 and pristine rr-PQT-12 by targeting sulphur are shown in Fig. 6.9. In pristine sulphur, $2p^{3/2}$ binding energy (B.E.) was observed at 163.8 eV. However, in AgNPs@rr-PQT-12, same was observed with blue shift of 0.4 eV and appeared at 164.2 eV. This again confirms the formation of fluorophore–plasmon coupled unified system of Ag NPs@rr-PQT-12 with silver nanostructures, by chemi-adsorption (through weak van der Waal forces), therefore partial charge transfer from rr-PQT-12 polymer backbone to Ag NPs take place and cause enhancement in BE of sulphur.

The partial charge transfer from polymer to Ag NPs cause generation of hole which induces enhancement in conductivity also. This again supports the coupling of surface plasmons of Ag NPs with the conducting polymer rr-PQT-12 [Pandey et al. (2015)].
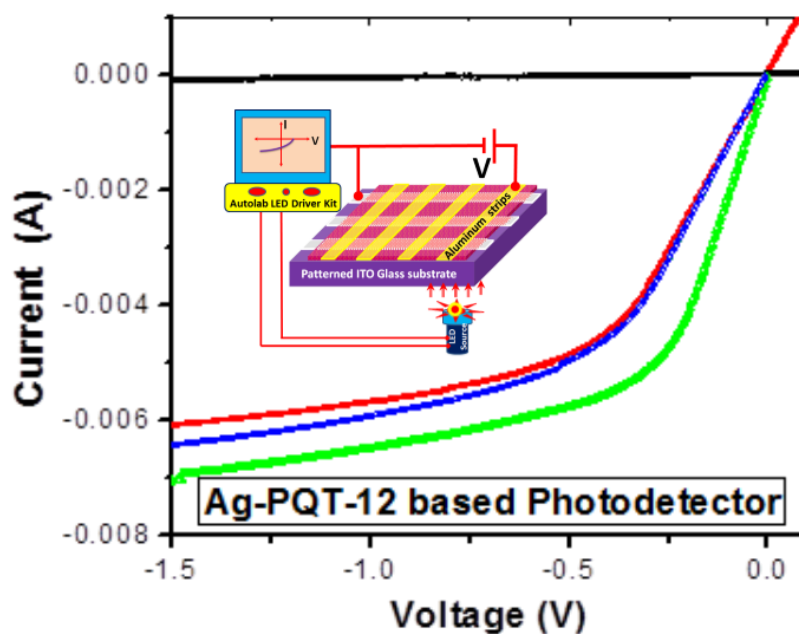
Fig. 6.8. J –V characteristics of AgNPs@rr-PQT-12 under illumination of different wavelength. Inset picture shows the device schematics.
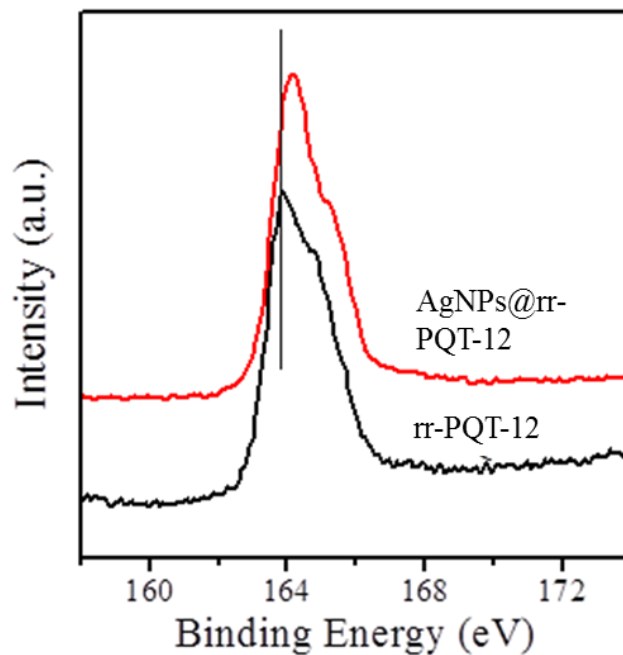

Fig. 6.9. X-ray photoelectron spectroscopy of pristine PQT and Ag@rr-PQT-12, respectively

6.4 Conclusions

We have explored the SPR coupled approach to enhance the photo generation of excitons while retaining their optical thickness. In order to explore this approach, a facile synthesis of Ag NPs surface plasmons resonance- regioregular Poly (3, 3′′′-didodecylquaterthiophene) (rr-PQT-12) coupled nano-composite have been conducted via FTM. The as-deposited thin film of nanocomposite was investigated via multiple characterization technique viz. morphological, spectral, morphological, and structural characterization for confirmation of formation of Ag NPs-polymer coupled nanocomposite thin film and compare with pristine polymer film. Finally, photovoltaic property of nanocomposite was examined via fabrication of sandwiched structure ITO/AgNPs@rr-PQT-12/Al by measuring photo-current using different wavelength of light which reveals the pretty good with wavelength dependent enhancement in photocurrent.